Magnetic induction assisted pyrolysis of plastic waste to liquid hydrocarbons on carbon catalyst

Cuong Duong-Viet, Lai Truong-Phuoc, Lam Nguyen-Dinh, Christophe Michon, Jean-Mario Nhut, Charlotte Pham, Housseinou Ba, Cuong Pham-Huu

Materials Today Catalysis 3 (2023) 100028

Contents lists available at ScienceDirect

Materials Today Catalysis

journal homepage: www.journals.elsevier.com/materials-today-catalysis

Magnetic induction assisted pyrolysis of plastic waste to liquid hydrocarbons on carbon catalyst

Cuong Duong-Viet [a], Lai Truong-Phuoc [a], Lam Nguyen-Dinh [b], Christophe Michon [c,*], Jean-Mario Nhut [a], Charlotte Pham [d,*], Housseinou Ba [e], Cuong Pham-Huu [a,*]

[a] Institute of Chemistry and Processes for Energy, Environment and Health (ICPEES) – UMR 7515 CNRS-University of Strasbourg, 25 rue Becquerel, 67087 Strasbourg Cedex 02, France
[b] Department of Chemical Engineering, The University of Da-Nang – University of Science and Technology, Da-Nang 550000, Viet Nam
[c] Laboratoire d'Innovation Moléculaire et Applications (LIMA) - UMR 7042 CNRS-University of Strasbourg, 25 rue Becquerel, 67087 Strasbourg Cedex 02, France
[d] SICAT SAS, 20 place des Halles, 67000 Strasbourg, France
[e] BLACKLEAF SAS, 210 rue Geiler de Kaysersberg, 67400 Illkirch, France

ARTICLE INFO

Keywords:
Waste plastic recycling
Carbon catalyst
Induction heating
Pyrolysis
Hydrocarbon production

ABSTRACT

Carbon-based catalyst can effectively crack model waste plastic based on polyolefins under contactless induction heating and yield gaseous and liquid hydrocarbons fractions at mild reaction temperatures. High catalytic performances are reached thanks to the stable catalyst bed temperature arising from the high heating rate of the induction setup. By comparison to indirect Joule heating which required much higher temperatures, contactless direct induction heating allows a compensation of the internal temperature loss during such highly endothermic process through direct heat targeting. The single carbon-based catalyst combined a high and stable activity with an extremely high stability as a function of cycling tests with pure or mixed polymers. By comparison to the acid or metal based catalysts used in plastic cracking, such low cost carbon catalyst avoids deactivation within cycling tests and therefore provides an efficient and cost-effective route for waste plastic recycling and also as chemical storage means for renewable energy.

1. Introduction

Plastics represent one of the main commodities for our societies in almost every domains spanning from industrial packaging to health care as well as composites for transportation or in different electronic devices [1]. The single-use of plastics, ca. 40%, as commodities represents one of the main sources for the CO_2 releasing and cause problems for environment and health, taken into account that nowadays, about 90% of waste plastic is dumped or landfilled while only a very small amount is recycled or converted into energy, i.e. recycling (9%) and incineration (12%) [2–4]. New legislations and environmental policy significantly foster plastic recycling in order to reduce the problem of waste disposal and to produce value-added products for transportation and petrochemical processes [5,6]. Plastic waste as such is contaminated with different dopants and thus, preliminary sorting and cleaning are necessary before initiating the recycling as the process efficiency also depends on the nature of the various additives used in the plastic [7]. Nowadays, depending on the quality and purity of the plastic waste different recycling processes are developed: (1) reuse (direct from the plastic waste), (2) reprocessing or mechanical recycling, (3) depolymerization to produce raw monomeric material (not applying for all types of plastics) which remains scarce [8], (4) thermochemical conversion of the waste plastic into hydrocarbon feedstock [9,10], and finally, (5) energy recovery through incineration. The net gain varies according to the type of recycling process employed as well as the catalysts used, but it is generally agreed that recycling plastics contributes to a significant reduction of carbon emissions, especially when it allows one to produce back raw monomer, i.e. closed-loop chemical recycling. Among these processes the thermochemical/catalysis route allows one to recycle waste plastic fractions that cannot be reused or recycled through mechanical or depolymerization processes and to avoid landfill or incineration. Thermochemical recycling, or catalytic pyrolysis process, allows one to reduce in a significant manner the greenhouse gas (GHG) emission compared to incineration [11] while remaining close, in terms of GHG, to the mechanical recycling as this later can only be applied to a very limited fraction of waste [12].

* Corresponding authors.
E-mail addresses: c.michon@unistra.fr (C. Michon), pham/@sicatcatalyst.com (C. Pham), cuong.pham-huu@unistra.fr (C. Pham-Huu).

https://doi.org/10.1016/j.mtcata.2023.100028
Received 22 August 2023; Received in revised form 21 September 2023; Accepted 2 October 2023
Available online 4 October 2023

Catalytic pyrolysis process (CPP) has received an ever growing interest for its flexibility in terms of processing contaminated plastics as well as waste plastics mixture which are not easy to be handled by mechanical recycling. Thanks to such advantages chemical recycling of waste plastic has significantly increased in recent years [4,13]. A large part of the different literature reports deals with the upcycling of waste polyolefins which accounted for ca. 55% of total municipal solid wastes [2,14]. They are mostly used in the production of plastic bags (low-density polyethylene, LDPE), rigid packaging, plastic pipes and bottles (high-density polyethylene, HDPE) or medical devices and laboratory equipment (polypropylene, PP). The conversion of such plastics into valuable liquid fuels and waxes represents a great promise in numerous industrial applications [15–17]. The efficiency of the CPP depends on several factors such as catalyst, reactor operating mode and process parameters, which will have a non-negligible influence on the operational cost of the process developed. All of these parameters can be controlled separately to optimize the final process. Until now, zeolite catalysts, especially ZSM-5, are the most employed catalysts due to their high cracking activity, relatively affordable cost and commercial availability [18–23]. Despite the relatively large number of studies most of them report catalytic performance using a relatively high catalyst to feedstock ratio which renders the direct comparison with industrial process difficult. In the case of metal-based catalysts most of the experiments were carried out under batch reaction conditions which could pose some problem for the scale-up of the process, i.e. catalyst recovery, lack of deactivation assessment as in the case of dynamic process [24]. In addition, the relative long reaction time process could also hinder the industrial development. The deactivation assessment, especially for zeolite-based catalysts, also renders the scale-up development not straightforward [18,25]. Indeed, during their use, the zeolite pores or supported metal catalysts could be partially or fully blocked by waxes-like or carbonaceous compounds which induce gradual deactivation [22,26]. The replacement of these acidic and metal-based catalysts by other catalysts with higher chemical resistance could represent a step forward in this process. Recent work by Sun et al. [27] and by Zhang et al. [28] described the chemical conversion of waste plastics via catalytic pyrolysis with activated carbons containing acid sites. The authors have shown that such carbon-based catalysts could provide a new path to convert waste plastics into high value-added liquid fuel for transportation. Recently, Duong-Viet et al. [29] have reported the efficient cracking of waste plastic into either light olefins or liquid fuel on metal- and acid-free carbon-based catalysts which display extremely high stability as a function of cycling tests thanks to the high chemical and thermal resistance of plain carbon material. It is thus of high interest to develop carbon-based catalysts for chemical recycling of waste plastic which could reduce the cost of the process. In addition, in case of complete fouling through gradual carbonaceous deposition the final composite can be re-used in other applications involving carbon material such as additives in the area of construction, transport or as soil amendment.

The CPP also requires energy to crack down the polymer into valuable end products being it gaseous monomers or liquid fuel for transportation or petrochemical processes. The traditional heating mode using fuel gas burners offers low heat transfer efficiency and a concomitant emission of large amount of GHG [30]. Therefore, it is of high interest to replace low thermal efficiency Joule heating mode by other ones with better heat efficiency and use of renewable energy instead of fossil one. Recently, it has been reported by different research groups that unusual catalytic processes can be carried out using direct induction heating (IH) in place of traditional heat convection/conduction transfer [31–37]. In such catalytic processes the heat is directly targeted to the solid catalyst without over heating the whole reactor volume and therefore reduces significantly the waste heat for the processes. The plastic cracking is also a very high endothermic process and thus, the possibility to maintain the reaction temperature during the process, thanks to the high heating rate of the induction system, is of high interest as it prevents the formation of long-chain hydrocarbons, i.e. waxes, due to the decrease of the reaction temperature along the reactor. Recently, induction heating has also been used by Luo et al. to operate catalytic deconstruction of medical waste to produce hydrogen-rich gases and graphite [38]. Alongside with magnetic compounds, which can be actively heated by IH, electrical conductors such as carbon-based materials could also be efficiently heated up by IH [39–43]. It is expected that the combination of carbon, an electrical conductor material, and direct induction heating of the catalyst could open up new investigation fields of heterogeneous catalysis where robust and low cost catalysts could be a game changer for operating old catalytic processes with improved efficiency. In addition, IH also represents a green heating mean for operating catalytic processes as it can be operated using exceeding renewable energy sources (RES), instead of traditional fuel or natural gas burners, for heating up the reactor which thus, contributes to the reduction of the GHG for chemical processes, i.e. electrification of chemical processes [44,46]. The use of RES to produce chemical products also represents a smart way to operate chemical storage of the excedental RES.

Some mild recycling processes have also been reported recently which deal with the use of either photothermal [45] or electrocatalytic [46] as well as enzymatic [47] processes for the conversion of polyolefin-based polymers back into chemicals and hydrogen. It is expected that such processes will greatly contribute to the improvement of the recycling of waste polymers and to reduce the associated carbon footprint of this sector.

Herein, we report a combination of high heat harvesting carbon-based catalyst and direct induction heating to crack down model polymers (HDPE and LDPE) into gaseous and liquid hydrocarbons at mild reaction temperature ($\leq$ 500 °C) [29]. The advantages of using carbon as catalyst are the following: low impact of impurities or carbon deposit on the catalyst stability, contrary to other sensitive active catalysts such as zeolite or metal and cost effective production and reutilization. The catalytic process was carried out in a continuous reactor which allows one to assess the stability of the catalyst in continuous operation mode and also to reduce the complexity for scale-up. The results indicated that carbon-based catalyst operated under direct IH mode displays high catalytic performances as well as long-term stability and could represent a viable alternative for the chemical recycling of waste plastic.

2. Experimental section

2.1. Mesoporous carbon-based materials

The catalyst used is a porous carbon in the form of extrudates carbon (MESOC+ produced by ACM GmbH, www.sicatcatalyst.com), produced at industrial scale of 40 tons per year, with the following dimension: diameter of 3 mm, and length up to 4–6 mm. The carbon catalyst was used as received without any pre-treatment. Elemental analysis (ICP-AES) carried out on the MESOC+ −3 catalyst confirms the high purity of the material. The most important impurities detected are S (250 $\pm$ 10 ppm) and Si (1100 $\pm$ 10 ppm) while the others, i.e. Ca, K, Na only contribute to ca. 60 $\pm$ 10 ppm each in the sample.

2.2. Feedstock

The different experiments were carried out by using model high- and low-density polyethylene (HDPE, Alcudia® 5503 and LDPE, Alcudia® 2308 F) chips (Repsol Ltd.). The chips are in the form of semi-spherical particles with an average diameter of ca. 3 mm and thickness of 2 mm.

2.3. Plastic conversion process

The representative setup used for the process is presented in Fig. 1 with associated legendary for different sections. The first section was consisting in a polymer supplier which can contain a polymer weight

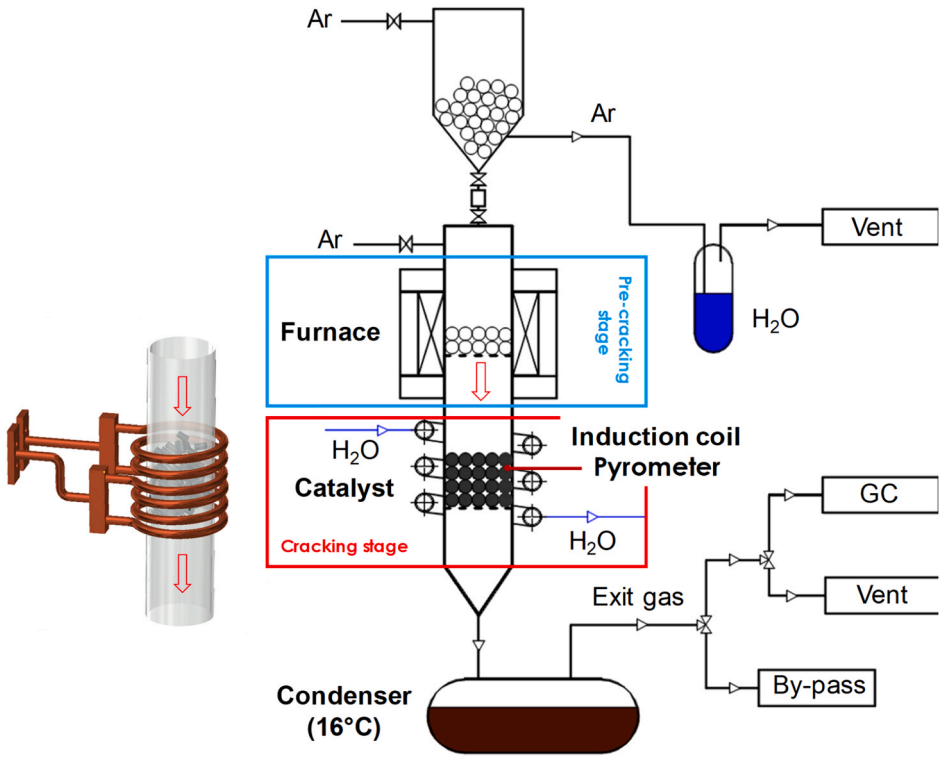

Fig. 1. Schematic presentation of the catalytic setup used for the upcycling of waste plastic into liquid hydrocarbon operated under contactless induction heating mode. Inset: schematic representation of the reactor localized inside the induction coil. Detail description of the pyrolysis process setup is presented in the SI section.

from 6 to 100 g. The reservoir was continuously flushed with an argon flow (30 mL. min^{-1}). The polymer chips were fed to a pre-cracking stage consisting with 4 g of silicon carbide (extrudates with diameter of 3 mm and length up to 4 mm) localized within an electric furnace kept at 470 °C and continuously flushed with an argon flow with a flow rate of 30 mL. min^{-1}. In the first pre-cracking stage the polymer was decomposed into smaller fragments, random cracking, to yield both gaseous and liquid compounds, which further passed through the connection pipe, maintained at 300 °C, into the second cracking stage operated either under direct IH or indirect Joule heating. The outgoing products, from the first pre-cracking stage, were also analyzed through direct cooling in order to get more insight about their nature. At room-temperature the products are in the form of waxy compounds which are hardly solubilized in petroleum ether solvent (see Fig. S1 of the SI); this indicates that the pre-cracking stage only crack down the pristine polymer into some long-chain fragments (mostly waxes at room temperature) which will be further cracked into liquid hydrocarbons in the second cracking stage.

The second cracking stage can be heated up either under direct IH or indirect Joule heating mode. The IH experiment was conducted on an EasyHeat® 8310 induction heating setup (10 kW, Ambrell Ltd) equipped with a spiral 6-turn induction coil ($L = 1.05$ m, pure coil resistance $= 2.066 \times 10^{-3}$ Ω) and external cooling chiller with recirculated water/glycerol (10%) mixture as cooling media. In a typical experiment, a quartz reactor containing the catalyst, similar to that used for the JH, was placed inside the induction heater coils (see inset in Fig. 1 and S2 in SI). The real-time temperature control/regulation was ensured by a PID system (Proportional Integral Derivative controller, Eurotherm model 3504) connected to a laser pyrometer (Optris®, power < 1 mW, located at ≈ 30 cm from the catalyst) focused on the middle of catalyst bed on the external wall of the quartz reactor and another for the monitoring of the entrance temperature (see Fig. S2 in the SI section) and with the capability of working in 150–1400 °C range. The heating/cooling rate of the system is about 2000 °C min^{-1} in the 160–600 °C temperature range which could allow the efficient temperature maintaining during the highly endothermic cracking process. It is worthy to note that the inductor operated at a frequency of 263 kHz which generated a much lower magnetic field compared to those operated at lower frequency, i.e., < 10 kHz. In order to reduce the exposure of the worker to the magnetic field the setup was localized inside a Faraday cage surrounded with metal mesh.

For conventional Joule heating the catalyst was loaded in a quartz reactor housed inside an electrical oven (ERALY Co., $\varnothing_{OD} = 200$ mm, $\varnothing_{ID} = 55$ mm, length = 300 mm, $I_{max} = 8.6$ A, $T_{max} = 1100$ °C). The reactor was housed inside a tubular electrical oven and both ends were insulated with quartz wool plugs. The catalyst was evaluated under the same conditions with the polymer decomposition at 450 °C in the first stage as described above for the IH mode. The temperature was measured by two thermocouples, one inserted inside the wall of the oven and one is attached to the external wall of the reactor. The direct insertion of the thermocouple inside the carbon bed should be avoided as the metal of the thermocouple could induce some parasite reactions. The reaction temperature (heating rate of 10 °C min^{-1}) was controlled by the thermocouple located next to the external wall of the reactor.

The reaction products exit from the cracking stage were further passed through a trap maintained at 16 °C for condensing the liquid hydrocarbons while the gaseous products were directed to the gas chromatography (GC) for analysis. It is worthy to note that under IH mode only the solid localized inside the induction coil was heated and the temperature after 30 mm from the carbon bed is about 50 °C. Such low exit temperature induces a rapid quenching of the high boiling point hydrocarbons in the exit stream leading to the formation of liquid hydrocarbons trickled down inside the reactor. The reaction products were analysed on-line by two VARIAN 3800 gas chromatographs. The first one equipped with two detectors (thermal conductivity detector (TCD) and a flame ionization detector (FID) connected to CP-Silica PLOT and CP-SIL5 CB columns) was used to analyse H_2/CH_4 and hydrocarbons up to C_{12}, respectively. The second one equipped with a FID detector connected to a Restek RT alumina BOND column, was employed to separate lighter hydrocarbons such C_2H_2, C_2H_4 and C_2H_6 and other hydrocarbons

up to C_7. Calibration curves were used to quantify CH_4, H_2, C_2, C_6H_6 and $C_{10}H_8$. The Dietz factor method was used for the calculation of other hydrocarbons using the areas of FID integration. The liquid hydrocarbons recovered in the trap were analysed using a PONA Silicon gum (50 m, 0.2 mm ID, 0.5 μm) column. The detail analysis processes and the representative chromatograms are presented in the SI section (Fig. S3 to S5).

2.4. Characterization techniques

Scanning electron microscopy (SEM) was carried out on a ZEISS 2600 F platform with a resolution of 5 nm. The sample was deposited onto a double face graphite tape in order to avoid charging effect during the analysis.

Transmission electron microscopy (TEM) analysis was carried out on a JEOL ARM-200F working at 200 kV accelerated voltage, equipped with a probe corrector for spherical aberrations, and a point-to-point resolution of 0.2 nm. The sample was dispersed by ultrasounds in an ethanol solution for 5 min and a drop of the solution was deposited on a copper covered with a holey carbon membrane for observation.

The *Brunaüer-Emmett-Teller* (BET) specific surface area (SSA) and the pore size distribution of the support and the catalyst, after thermal treatment, were determined by liquid N_2-adsorption and desorption on an ASAP 2020 Micromeritics® instrument. All the samples were degassed at 250 °C under vacuum for 8 h in order to remove all the moisture. The pore size distribution was calculated from the desorption branch of the isotherm using the Barrett Joyner Halenda (BJH) approach.

Thermal gravimetric analysis (TGA) was realized on a TGA Q5000 instrument with a heating rate of 10 °C•min^{-1} under air flow at atmosphere (20 mL•min^{-1}). The weight of the sample was kept at around 10 mg in order to avoid diffusion problems during the analysis.

Powder X-ray diffraction (PXRD) measurements were carried out on a D8 ADVANCE Bruker diffractometer with a Cu Kα X-ray source ($\lambda = 1.5406$ Å). Rietveld refinements are performed using GSAS-II software. The mean size of ordered (crystalline) domains (τ) is calculated from the Debye−Scherer equation: $\tau = K\lambda/\beta \cos\theta$, where K is a shape factor, λ is the X-ray wavelength, β is the line broadening at half the maximum intensity (FWHM), and θ is the Bragg angle.

Raman spectra were recorded on LabRAM ARAMIS Horiba Raman spectrometer equipment. Spectra were acquired in the 500–4000 cm^{-1} range at the laser excitation wavelength of 532 nm.

^{1}H (400 MHz), ^{13}C (100 MHz), ^{1}H-^{1}H COSY and ^{1}H-^{13}C HSQC NMR spectra were acquired on Bruker Advance III spectrometers. The chemical shifts are referenced to the residual deuterated or ^{13}C solvent peaks. Chemical shifts (δ) and coupling constants (*J*) are expressed in ppm and Hz respectively.

3. Results and discussion

3.1. Carbon-based material characteristics

The mesoporous carbon (MESOC+−3) was used in the form of extrudates with the following dimension, diameter, 3 mm, average length, 4–6 mm (Fig. 2 A). The surface of the carbon catalyst is relatively rough as evidenced by the low magnification SEM micrograph and is constituted by a dense porous network of macro- and mesopores according to the high resolution SEM micrograph (Fig. 2B) and N_2 chemisorption. It is expected that such macropores could act as channels to allow the reactant to get access to the porous network localized within the sample matrix, i.e. meso- and micropores, to initiate cracking process. TEM analysis shows the presence of carbon nodules with an average diameter of ca. 50 nm with turbostratic structure with a low graphitization degree and linked each other to generate such porous structure (Fig. 2 C to E).

The specific surface area of the carbon material, measured by N_2 adsorption at liquid N_2 temperature, amounted to 320 m^2. g^{-1} constituted by 115 m^2/g of mesopores and 205 m^2/g of micropores (Table 1). The carbon catalyst displays an apparent electrical conductivity of about 50 S. m^{-1}. The average particle size determined by the Debye-Scherer equation is centered at around 30 ± 5 nm.

Table 1
Specific surface area of the MESOC+ −3 catalyst, fresh and spent, after pyrolysis under IH and JH modes. The amount of solid residue deposited on the spent catalyst is also reported for comparison.

	Fresh catalyst	Spent catalyst[a]	Spent catalyst[b]
	JH mode		
SSA[c] (m^2.g^{-1})	320	15[d]	-
Solid residue deposit (wt%)	-	12	-
	IH mode		
SSA[c] (m^2.g^{-1})	320	14[e]	8[f]
Solid residue deposit (wt%)	-	10	26

[a] Spent catalyst after pyrolysis of 20 g of model HDPE polymer
[b] Spent catalyst after pyrolysis of 140 g of model HDPE/LDPE polymer
[c] Specific surface area measured by BET method using N_2 adsorption at liquid nitrogen temperature
[d] After reaction at 600 °C with 20 g of model HDPE
[e] After reaction at 500 °C with 20 g of model HDPE
[f] After reaction at 500 °C with 140 g of model HDPE/LDPE mixed polymer

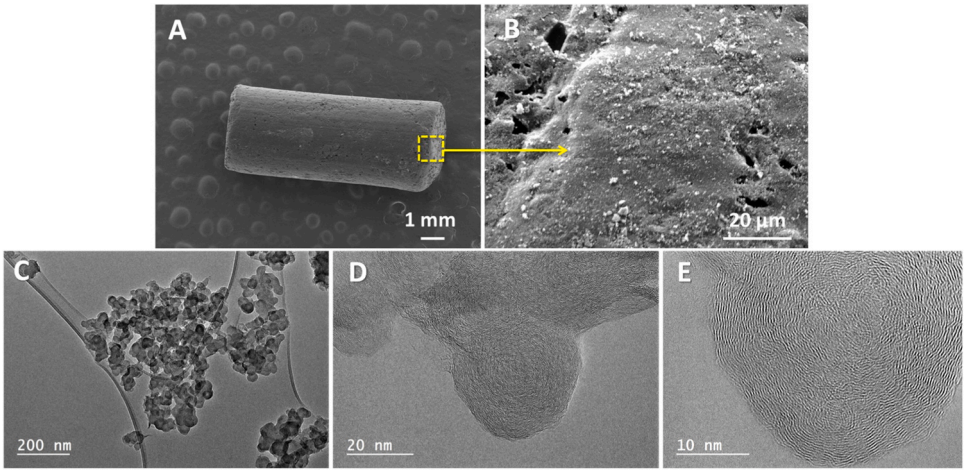

Fig. 2. (A, B) SEM and (C, D) TEM micrographs of the pristine MESOC+ −3 carbon catalyst with different magnifications. (E) High-resolution TEM micrograph showing the microstructure of the onion-like carbon nanoparticle with structural defects on the outer graphene layers.

The XPS survey and C1s spectra of the carbon catalyst confirm the presence of only C and O on the sample surface (Fig. 3 A and B). Oxygen atoms are present in the form of oxygenated functional groups, such as –OH, -C═O and –CO, linked with the carbon ones, i.e. defective sites (Fig. 3B). The TGA spectrum recorded on the carbon catalyst is presented in Fig. 3 C and confirms the relatively low ordered structure of the material which is in good agreement with the TEM results presented before. The TGA spectrum indicates that the carbon was completely consumed at temperature around 650 °C in air (Fig. 3 C). The sharp shape of the DTG curve also confirms the high kinetic of the combustion process and the presence of a unique type of carbon inside the sample. The residual acidic site on the MESOC+ −3 catalyst was also analyzed and the corresponding NH_3-TPD spectra is presented in Fig. 3D. The same analysis was also carried out on a zeolite sample for comparison. According to the results the carbon catalyst contains almost no acidic sites and the small NH_3 adsorbed could be ascribed to some reaction of functional groups on the catalyst surface.

The graphitization degree of the pristine and spent carbon samples

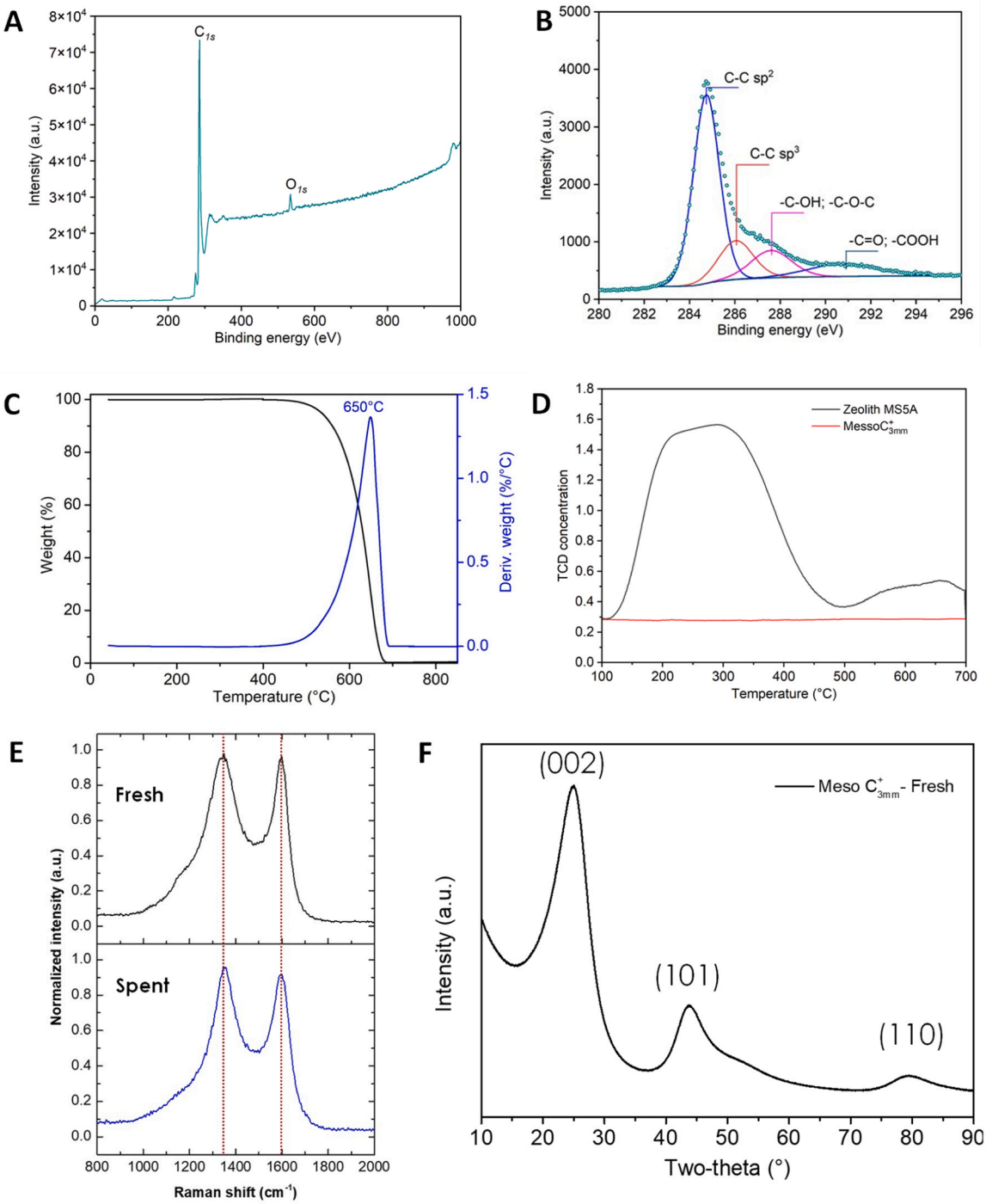

Fig. 3. (A) Survey XPS spectrum of the MESOC+ −1 sample. (B) High-resolution XPS C1s spectrum showing the presence of oxygenated functional groups. (C) TGA spectrum of the MESOC+ −3 carbon material (experiment was carried out under air with a flow rate of 20 mL. min^{-1} and under a heating rate of 10 °C. min^{-1}). (D) NH_3-TPD spectra of the MESOC+ −3 as received and a Zeolith MS5A for the benchmark. (E) Raman spectra of the fresh and spent carbon materials and (F) XRD pattern of the pristine carbon sample with broad diffraction lines.

was also determined by Raman and XRD techniques and the results are presented in Fig. 3E and F. The Raman spectrum of the pristine carbon sample displays a relatively large and high D peak compared to the G peak. The D and G bands are located at 1349 and 1596 cm^{-1}, respectively, on the fresh carbon sample (Fig. 3E). The D band is originating from disorder in the carbon structure [48] while the G band is associated with ideal graphitic lattice [49]. The I_D/I_G ratio is accounted for 1.31 which indicates that disordered carbon with low graphitization degree and high defects is predominantly present in the sample. Such results are in good agreement with those obtained by TEM and TGA analyses. On the Raman spectrum recorded on the spent catalyst, after reaction at 500 °C, the D band remains high which indicates that the deposited carbon displays a similar disordered structure as that of the pristine sample. XRD pattern of the pristine carbon sample displays a very broad diffraction lines at 25°, 44° and 78° of two-theta angle which confirms the low graphitization degree of the carbon sample (Fig. 3 F). The XRD pattern of the spent carbon sample after reaction at 500 °C (not shown) displays a very similar feature which is in good agreement with the fact that at such medium temperature (≤ 500 °C) carbon is mostly deposited in the form of low-ordered structure.

3.2. Waste plastic cracking process

3.2.1. Influence of the reaction temperature and heating mode

The catalytic performance of the MESOC+ −3 (3 mm in diameter), operated under traditional indirect Joule heating using an electric oven, for converting model HDPE into gaseous and liquid hydrocarbons as a function of the reaction temperature is presented in Fig. 4. According to the results medium reaction temperature, i.e. 500 °C, only produces a small amount of gaseous fraction while the liquid fraction is exclusively constituted with long chain wax-like hydrocarbons (Fig. 4 A). Increasing the reaction temperature to 550 °C leads to a slight increase of the gaseous fraction vs liquid/wax one, despite this later remains majority in a waxy state (Fig. 4B and digital photo in inset). At reaction temperature of 600 °C the gaseous fraction and the hydrocarbon chain length in the liquid fraction significantly increase and is mostly constituted with long chain carbon fraction ranged from C_{10} to C_{34} with mostly saturated fraction. However, it is worthy to note that despite the bond scission was increased at high cracking temperature the amount of methane remains low in the products at ca. 5 wt% which could be attributed to the absence of acidic centers on the catalyst. The proportion of light olefin fraction also slightly increases at high temperature indicated the existence of C-H bond breaking (Fig. 4 F). Such cracking behavior could be attributed to the presence of –OH, -C═O and –CO functional groups (as detected by XPS) on the carbon surface similar to that reported, using

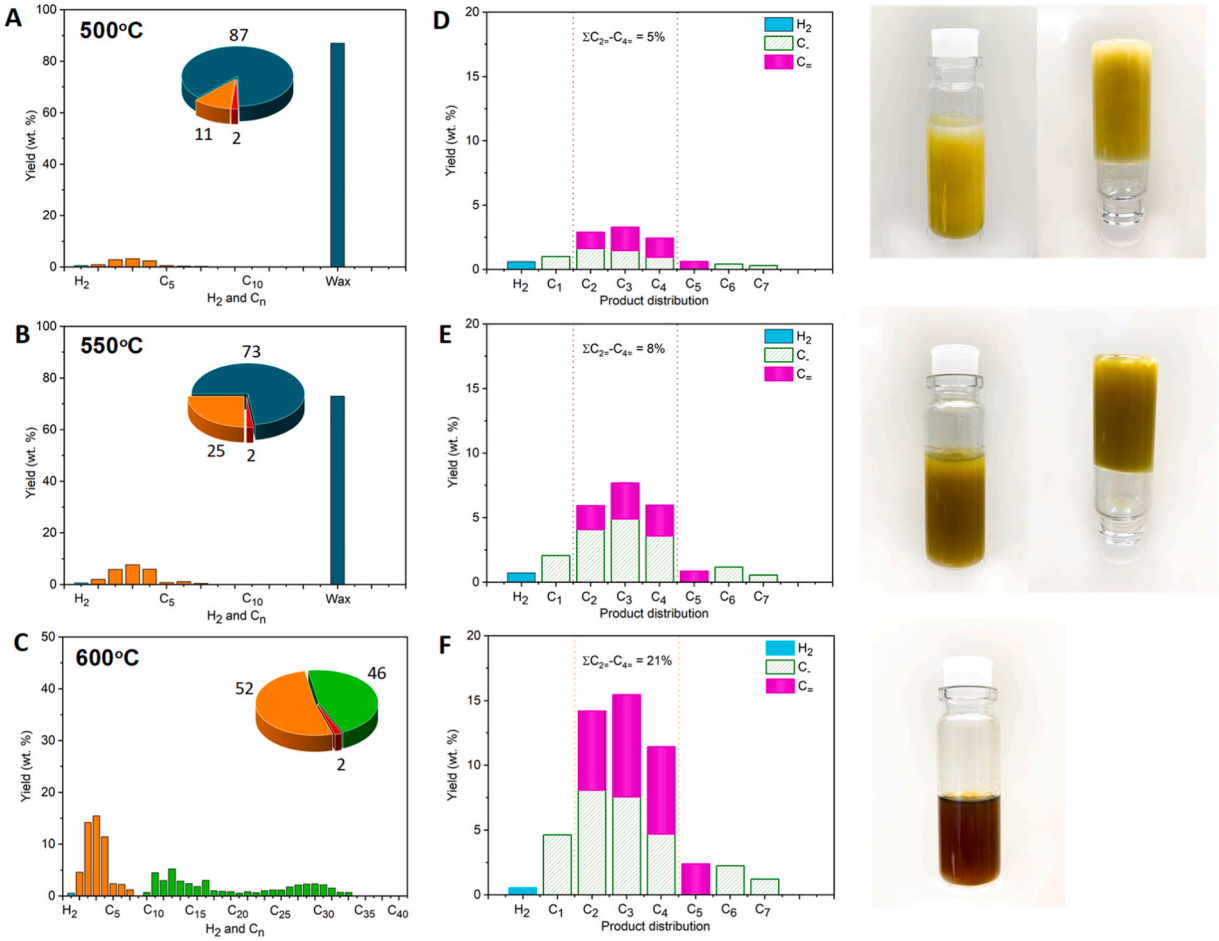

Fig. 4. Plastic-to-Fuels (PTF) process (selectivity wt%) using model HDPE polymer on 3 mm pellets of MESOC+ material under indirect Joule heating mode at various reaction temperatures (500, 550 and 600 °C). Products distribution (H_2 and C_n present in gaseous, liquid and solid waxes): (A, D) 500 °C, (B, E) 550 °C, (C, F) 600 °C. Fraction distribution: (peacok blue) Waxes, (orange) Gaseous, (green) Liquid, (red) Residue. Digital photos of the waxes and liquid hydrocarbons recovered are presented in the same figure for comparison. Reaction conditions: HDPE weight = 20 g with discontinuous feeding (10 g. h^{-1}), MESOC+ weight = 6 g (7 cm^3 in apparent volume), reactor diameter = 26 mm, argon flow rate = 30 mL. min^{-1} (STP), HDPE vaporization temperature at the first stage with an electric oven set at 450 °C. The liquid fraction was condensed in a trap keep at 10 °C using an external ice bath.

infrared technique, by Zhang et al. [28]. These results clearly evidence the low polyolefin cracking ability of the MESOC+ −3 operated under indirect JH mode which could be attributed to the problem of temperature stability during the highly endothermic cracking process of long-chain plastic (see discussion below). It is also worthy to note that the color of the waxes/liquid changes as a function of the reaction temperature, passing from yellow bright to yellow grey and finally, to dark brown (see photos in Fig. 4). Such color change could be related to the increase of some olefins and aromatics inside the product which are favored at high temperature. The detailed analysis will be carried out further using HSQC NMR technique (see vide infra and the Supporting Information).

On the other hand, the same carbon catalyst operated under direct induction heating, at reaction temperature ≤ 500 °C, mostly produces gaseous and short to medium carbon chain liquid hydrocarbon fraction (Fig. 5 A to C and digital photos in inset). Low viscosity liquid hydrocarbon was obtained alongside with some waxes at the lowest cracking temperature of 450 °C. At reaction temperature higher than 450 °C waxes are no longer detected and only short chain hydrocarbons was observed (Fig. 5B and C). The hydrocarbon chain distribution within the liquid fraction obtained at cracking temperature of 480 and 500 °C contains mostly carbon compounds with chain length shorter than C_{25} (Fig. 5B and C). Contrary to that observed with the JH mode the IH mode mostly yields short to medium hydrocarbons chain length, i.e. C_9 to C_{20}, at cracking temperature ≤ 500 °C, constituted mostly by saturated and a small amount of branched molecules. Similar to the results observed before the liquid fraction color is also changed from limpid yellow bright at 480 °C to slightly dark ones as increasing the reaction temperature indicating the presence of some olefins or aromatics inside the fraction. However, at such relatively low reaction temperature and in the absence of any acid sites on the catalyst surface the aromatics formation is unlikely to occur. The difference in terms of

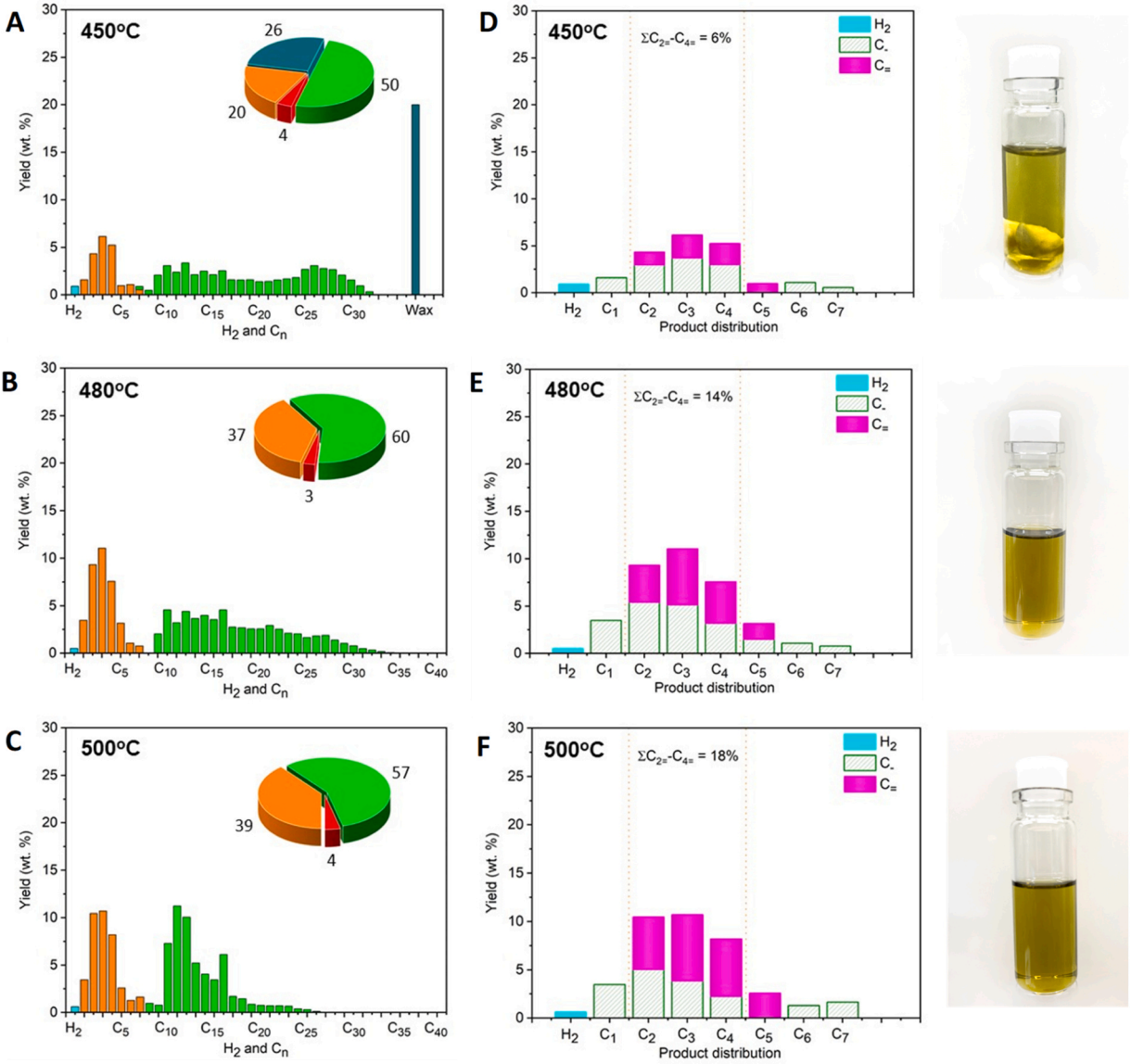

Fig. 5. Plastic-to-Fuels (PTF) process (selectivity wt%) using model HDPE polymer on 3 mm pellets of MESOC+ material under direct induction heating mode (450, 480, and 500 °C). Products distribution (H_2 and C_n present in gaseous, liquid and solid waxes): (A, D) 450 °C, (B, E) 480 °C, (C, F) 500 °C. Fraction distribution: (peacock blue) Waxes, (orange) Gaseous, (green) Liquid, (red) Residue. Digital photos of the waxes or liquid hydrocarbon recovered are presented in the same figure for comparison. Reaction conditions: HDPE weight = 20 g with discontinuous feeding (10 g. h^{-1}), MESOC+ weight = 6 g (7 cm^3 in apparent volume), reactor diameter = 26 mm, argon flow rate = 30 mL. min^{-1} (STP), HDPE vaporization at the first stage with an electric oven set at 450 °C. The liquid fraction was condensed in a trap keep at 10 °C using an external ice bath.

liquid fraction color between the JH and IH also support such hypothesis. Zhang et al. [21] and Zhang et al. [50] have reported that aromatic compounds significantly increase with increasing the cracking temperature which is related to the enhancement of the aromatization/cyclization of light alkane radicals on the acid sites of ZSM-5 catalyst.

The percentage of the different hydrocarbon fractions, i.e. gas, liquid, waxes, and solid residue deposited on the spent catalyst, obtained at various reaction temperatures and under both heating modes is summarized in Table 2. The direct comparison between the two heating modes at reaction temperature of 500 °C clearly evidences the advantage of using IH vs indirect Joule heating (Table 2). At 500 °C Joule heating process yields mostly waxes (87 wt%) and the gaseous fraction only contributes to about 11 wt% while under IH the product of the pyrolysis is mostly constituted by liquid and gas fraction (57 and 39 wt %, respectively) with a contribution of about 18 wt% of C_2 to C_4 light olefins. Among the liquid fraction the C_6-C_{16} fraction also contributes to about 52 wt% with mostly linear alkanes according to the ^{13}C NMR analyses (Fig. S17, S22, S27). Such results are interesting as for some post-process upgrading the presence of olefins and/or aromatics needs to be avoided.

The ^{1}H NMR spectra of the different liquid fraction obtained as a function of the reaction temperature and heating mode, i.e. 600 °C under JH and 480 °C under IH, are presented in Fig. 6 (See the Supporting Information for detailed 1D and 2D NMR characterizations Fig. S6-S15). The liquid products obtained at 600 °C in the JH mode contain a large amount of linear saturated and branched alkanes and alkenes as well as some aromatics compounds, a moderate isomerization of aliphatic compounds being observed by comparison to other report [26] (Fig. 6 A). The low aromatic compounds detected in the liquid fraction could be directly linked with the lack of acidic sites on the catalyst surface as suggested before. Similar trend is also observed for the sample recovered from IH mode with, however a lower ratio between aromatic and aliphatic compounds than the one obtained with the JH mode, i.e. 1/17 versus 1/15. It is expected that the low cracking temperature used under IH mode contributes to the reduction of the aromatics formation in the liquid fraction product. For both heating mode, alkene compounds appeared to be a mixture of terminal and internal derivatives in a 2–1 ratio (See Fig. 6 and the SI section). The branched alkane/alkene could be formed on oxygenated functional groups with weak acidity.

Table 2
Plastic-To-Fuel performance on MESOC+ −3, operated under direct induction heating and indirect Joule heating mode, catalyst using HDPE as model waste polymer as a function of the polymer charge. Reaction conditions: polymer weight feeding = 10 g. h^{-1} with discontinuous feeder, MESOC+ weight = 6 g (with an apparent volume of 7 cm^3), reactor diameter = 26 mm, argon flow rate = 30 mL. min^{-1}, reaction temperature = 500 °C, HDPE vaporization at the first stage with an electric oven set at 470 °C. The liquid fraction was condensed in a trap keep at 10 °C using an external ice bath.

	Indirect JH			Direct IH		
	500	550	600	450	480	500
Products yields (wt%)						
Liquid	0	0	46	50	60	57
Gas	11	25	52	20	37	39
Waxes	87	73	2	26	0	0
Solid residue	2	2	0	4	3	4
Gas composition (mol%)						
H_2	0.6	0.7	0.6	0.9	0.5	0.6
CH_4	1.0	2.1	4.6	1.6	3.5	3.5
C_2H_4	1.2	1.9	6.1	1.4	3.9	5.4
C_2H_6	1.5	4.1	8.1	3.0	5.4	5.0
C_3H_6	1.7	2.8	7.9	2.4	5.9	6.9
C_3H_8	1.4	4.9	7.6	3.7	5.1	3.9
Others (> C_3)	3.6	8.6	17.3	7.9	12.6	13.7
Liquid distribution (mol%)						
C_6-C_{16}	0	0	27.2	22.8	31.9	52.2
C_{16}-C_{23}	0	0	9.1	13.4	18.2	6.9
Heavy HC and waxes (> C_{23})	87	73	17.3	45.7	11.8	0.9
Ratio aromatic / aliphatic[a]	-	-	1/15	-	1/17	1/14

[a] Determined from the NMR analysis

The difference in terms of catalytic performance, between the two heating modes, could be attributed to the ability of the IH mode to target directly the heat to the catalyst and to maintain the reaction temperature during the cracking process thanks to the fast temperature feedback of the laser pyrometer and the high heating rate delivered by the induction coil. Indeed, the polymer cracking process is a high endothermic reaction which could significantly lower the catalyst surface temperature during the cracking process. In the case of indirect JH mode, the high inertia of the oven to provide heat to the catalyst bed could be at the origin of a reaction temperature decrease during the cracking process and thus, leads to the formation of long chain hydrocarbons or even waxes as observed. By comparison, as explained above the direct IH mode allows the efficient maintain of the catalyst bed temperature during the process to operate kinetically the cracking process similarly to that reported for microwave heating mode used in other catalytic processes [51,53]. Such on-the-spot temperature regulation has also been reported in the case of other endothermic or exothermic reactions such as steam/dry reforming or CO_2 methanation where heat management plays a crucial role [40,42,52].

The way the catalyst is heated could also be advanced to explain the results obtained between the two heating modes. The schematic representation of the cracking process between JH and IH modes is presented in Fig. 7. In the case of indirect JH, the polymer vapors first coat the catalyst particles which could initiate some temperature loss due to both adsorption and vaporization of the hydrocarbon layer when getting in to contact with the catalyst surface. In a traditional JH mode, heat transfer typically takes place from the outer surface of the particle to the inside which could first evaporated the coating polymer layer before heating up the catalyst to initiate the cracking process and thus, only very marginal long-chain hydrocarbon was breakdown (Fig. 7 A). On the contrary, under direct IH mode the heat is rapidly generated inside the catalyst particle, as the coated hydrocarbon layer is not sensitive to IH, which could allow a fast initiation of the cracking process as soon as a layer of hydrocarbon was deposited on the catalyst surface (Fig. 7B). The high heat supply rate through the IH coil also greatly contributes to the catalyst bed temperature maintaining and, as a consequence, reduces the formation of heavy hydrocarbons or waxes as encountered with indirect Joule heating. Similar results are also obtained under microwave heating for plastic recycling into hydrogen and solid carbon as reported by Chen et al. [53] where the heat was generated inside the catalyst particles with a high heat supply rate. Similar explanation has also been proposed by Jie et al. [54] in a one-step microwave assisted process to convert plastic into hydrogen and carbon using $FeAlO_x$ as both heat susceptor and catalyst. Under microwave irradiation the catalyst is rapidly heated up to the set temperature while the plastic remains at lower temperature due to its transparency to incident microwave. The heat accumulates on the surface of the iron-based catalyst triggers the destruction of the adsorbed plastic to produce hydrogen and solid carbon. A recent study by Malhotra et al. [55] on the heat distribution inside the catalytic reactor operated under localized microwave heating had reported that the high heat supply allows the fast heating of the reactant flow, entering at room temperature, through rapid gas-solid heat exchange and after the reaction starts, the temperature is maintained thanks to the high heating rate of the microwave in a very similar way as that involved under direct IH [56]. The same heating scheme cannot be carried out using indirect Joule heating due to the inability of the indirect boundary heating to maintain the temperature of the catalyst due to its low thermal inertia.

The SSA of the spent catalyst, operated under direct IH and indirect JH, are reported in Table 1 and compared with that of the fresh catalyst. The presence of additional carbonaceous residue was also analyzed by weighting the spent catalyst and compared with the pristine one. According to the results the SSA of the carbon sample significantly

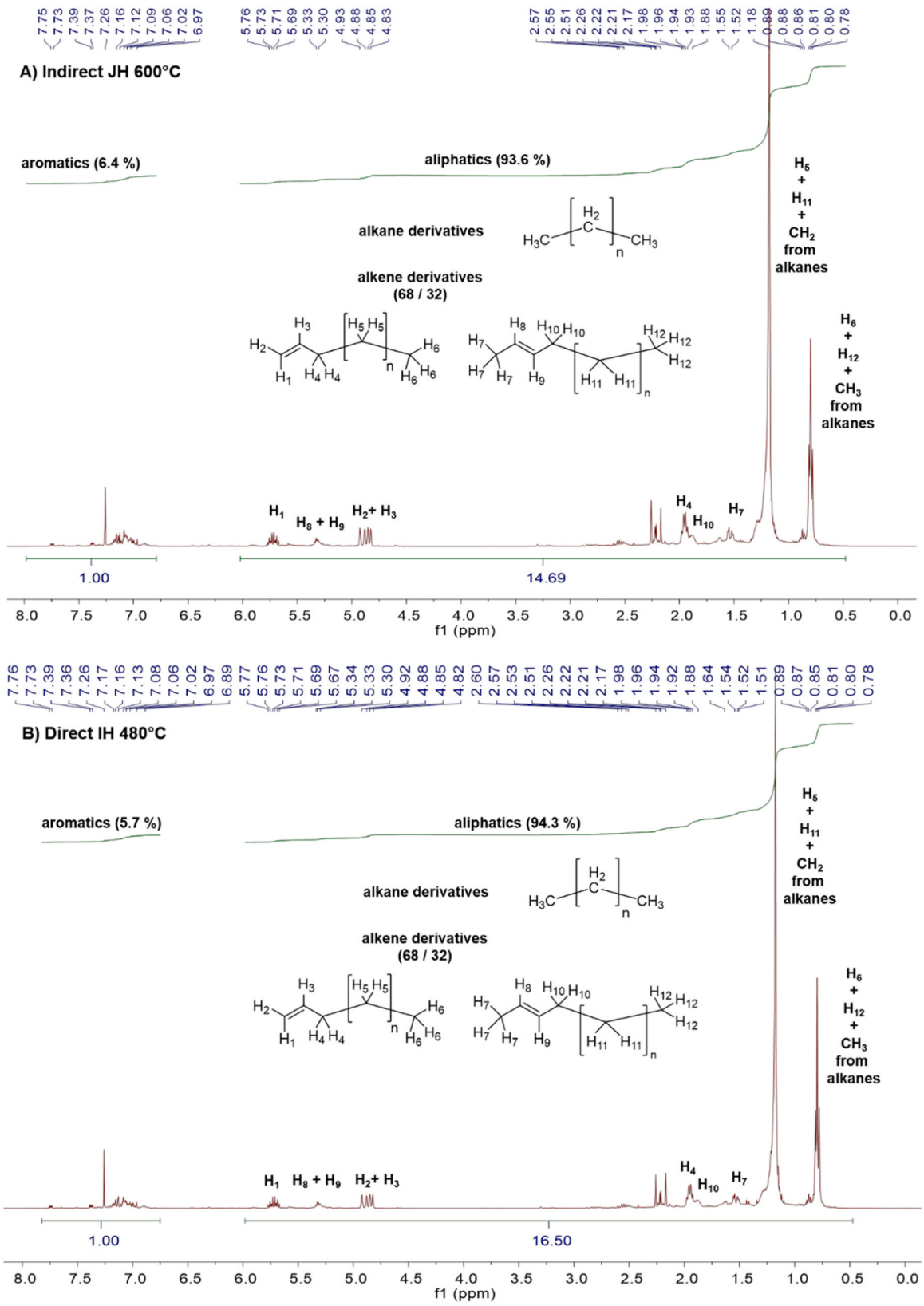

Fig. 6. ^{1}H NMR spectra of the liquid fraction obtained as a function of the reaction temperature, i.e. 600 (A) and 480 °C (B), operated under indirect JH and direct IH modes. Reaction conditions: HDPE weight = 20 g with discontinuous feeding (10 g. h^{-1}), MESOC+ weight = 3 g, reactor diameter = 26 mm, argon flow rate = 15 mL. min^{-1}, HDPE vaporization temperature = 450 °C.

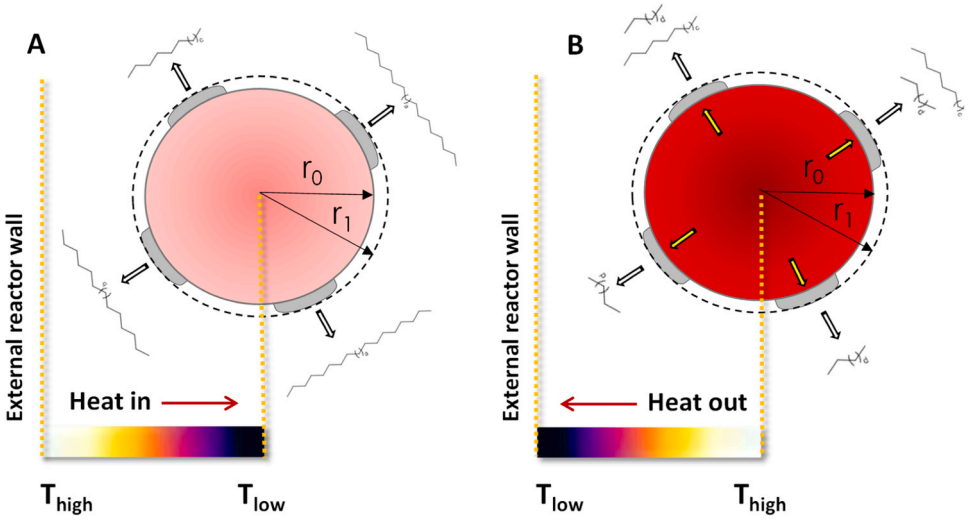

Fig. 7. Schematic representation of the heat transfer path between the reactor external wall and a single catalyst particle operated under indirect Joule (A) and direct induction (B) heating modes during the polymer degradation process. In the indirect Joule heating the heat is transferred from the oven to the reactor wall and then to the catalyst while in the direct induction heating the heat is generated inside the catalyst bed and transferred from the bed to the reactor wall.

decreased, passing from 320 to 14 m^2. g^{-1}, after the reaction with 20 g of polymer. Such SSA loss could be attributed to the porosity blockage by some solid carbonaceous residue, i.e. 10 wt% (Table 1).

3.2.2. *Long-term recycling test*

The long-term recycling test was conducted in a semi-continuous mode with a feeding rate of 10 g. h^{-1}, using HDPE as model feed at a reaction temperature fixed at 500 °C and with a carrier argon gas flow rate of 15 mL. min^{-1}. Each cycle refers to the conversion of 20 g of model plastic. The different product fractions, i.e. gaseous and liquid, are monitored at different time intervals and summarized in Fig. 8. The liquid fraction in the second cycle, after converting 40 g of HDPE, is significantly increases compared to that obtained on the first cycle (Fig. 8B vs 8 A and in Table 3). Such results could be attributed to some pore plugging, probably by some heavy hydrocarbons produced during the process, according to the drastic SSA loss (drop from 320 m^2/g down to 15 m^2/g), during the first cycle which could reduce the secondary cracking reactions. Similar results have also been reported by Du et al. [26] during batch cycling tests on tandem catalyst, zeolite and Ru supported catalyst, for the hydrogenolysis-isomerization of waste polyolefin

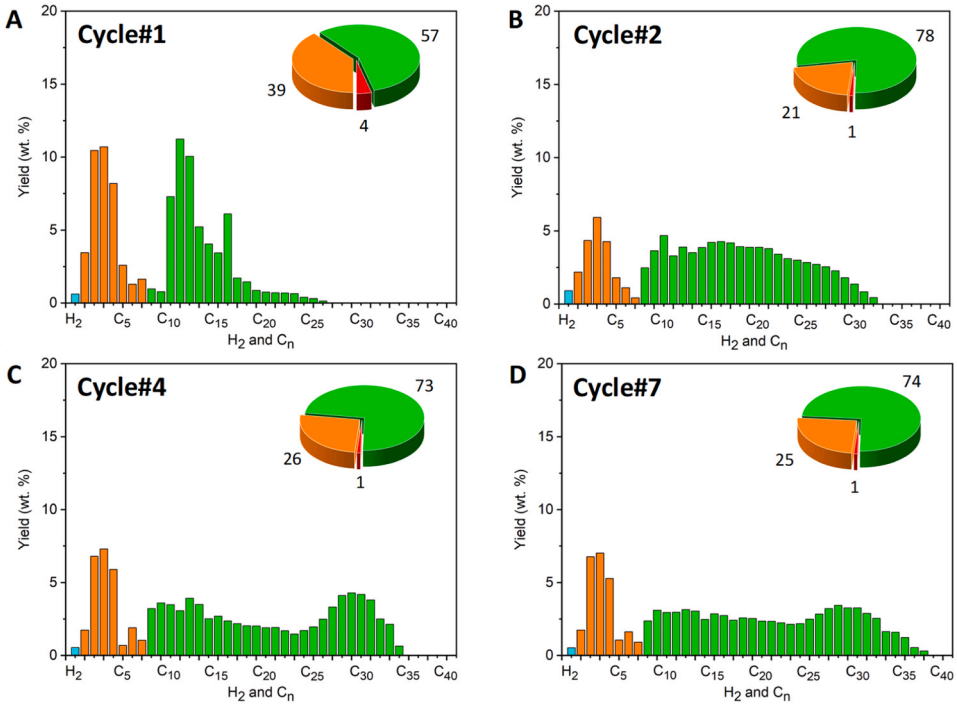

Fig. 8. Cycling tests for the plastic-to-Fuels (PTF) process using model HDPE polymer on 3 mm pellets of MESOC+ material under direct induction heating mode at 500 °C. Products distribution (H_2 and C_n present in gaseous, liquid and solid waxes) at 500 °C: (A) Cycle#1, (B) Cycle#2, (C) Cycle#4, (D) Cycle#7. Fraction distribution: (peacock blue) Waxes, (orange) Gaseous, (green) Liquid, (red) Residue. Reaction conditions: HDPE weight feeding rate = 10 g. h^{-1} with semi-continuous feeding, MESOC+ weight = 6 g, reactor diameter = 26 mm, argon flow rate = 15 mL. min^{-1}, HDPE vaporization at the first stage with an electric oven set at 450 °C. The liquid fraction was condensed in a trap keep at 10 °C using an external ice bath. Each cycle corresponding to 20 g of HDPE converted.

Table 3
Plastic-To-Fuel performance on MESOC+ −3, operated under direct induction heating, catalyst using HDPE as model waste polymer as a function of the polymer charge. Reaction conditions: polymer weight feeding = 10 g. h^{-1} with discontinuous feeder, MESOC+ weight = 6 g (with an apparent volume of 7 cm^3), reactor diameter = 26 mm, argon flow rate = 30 mL. min^{-1}, reaction temperature = 500 °C, HDPE vaporization at the first stage with an electric oven set at 470 °C. The liquid fraction was condensed in a trap keep at 10 °C using an external ice bath.

Cycling test	1	2	4	7
Time-on-stream (h)	2	4	8	14
Plastic converted (g)	20	40	80	140
Solid residue deposited (wt.-%)	10	12	16	24
Products yield (wt%)				
Liquid	57	78	73	74
Gas	39	21	26	25
Residue unrecovered in the reactor	4	1	1	1
Gas composition (mol.%)				
H_2	0.6	0.9	0.6	0.5
CH_4	3.5	1.9	1.8	1.7
C_2H_4	5.4	0.8	3.8	4.0
C_2H_6	5.0	2.9	3.0	2.8
C_3H_6	6.9	1.7	5.0	4.9
C_3H_8	3.9	3.3	2.3	2.1
Others (> C_3)	13.7	6.5	9.6	8.9
Liquid distribution (mol.%)				
C_6-C_{16}	52	35	31	28
C_{16}-C_{23}	7	26	13	17
Heavy HC (> C_{23})	1	18	31	31
Ratio aromatic/aliphatic (wt./wt%)	7/93	-	2/98	1/99

(LLDPE) to multibranched liquid alkanes. The authors have observed that the fraction of liquid products gradually increases as a function of the cycling tests while after fourth cycle, insoluble waxes becomes predominant, ca. 57%. They attributed such deactivation to coke or carbonaceous residue deposited on the catalyst which blocks the Brønsted acid sites and the metal active center. In our case, the catalyst contains neither acid site nor metal center and thus, the change of the liquid fraction was explained by a simple pores plugging which could decrease the contact time between the reactant and the catalytic active centers. Such tendency seems to continue before reaching a steady-state after Cycle#7 as shown in Fig. 8 C and D. It is worthy to note that the solid residue deposited on the catalyst remains low as a function of the cycling tests. The SSA of the carbon sample after the cycling tests only slightly decreases, passing from14 to 8 m^2. g^{-1} (Table 1).

The results clearly evidence the high stability of the MESOC+ −3 carbon-based catalyst for converting waste plastic into hydrocarbons with a throughput of ca. 24 g_{HDPE}. $g^{-1}_{catalyst}$ corresponding to 140 g of HDPE converted for 6 g of catalyst. According to the results one should also expect a high stability for additional tests. The relative stable hydrocarbon distribution at different time interval also confirms the high stability of the catalyst for the cracking of the polymer. It is worthy to note that the hydrocarbon chain length slightly increases as a function of the cycling tests which could be attributed to some pore plugging by carbonaceous residue which is in good agreement with the loss of the SSA between the fresh and spent catalyst reported above.

However, the amount of carbonaceous residue inside the catalyst remains stable after three cycles, 10 wt% relative vs the catalyst mass after the first cycle and 2 wt% for each following cycle, despite the large amount of waste plastic converted per weight of catalyst which indicates that deactivation by carbon fouling remains low vs the total amount of converted plastic. Muley et al. [57–59] have reported that carbon deposition is much more reduced when operating the catalytic reactions under induction heating. Wu et al. [60] have observed that large amount of carbon was deposited onto the Ni-CaO-C catalyst surface after biomass steam gasification operated under traditional indirect convection/conduction heating while little carbon deposit was observed for the one operated under direct IH mode. The authors have attributed such results to a positive gradient temperature across the catalyst surface, and also between the catalyst and the surrounding gas-phase medium, similarly to that reported by other research groups operating with microwave heating mode [61], which prevents the adsorption and polycondensation of product molecules that generate carbonaceous residue. In addition, it is worthy to note that as the catalyst is constituted by carbon, and thus carbon deposited during the process will not induce any chemical deactivation problem unlikely to zeolite or supported metal catalysts where deactivation by carbon coverage of the active sites localized in the zeolite pores is a main drawback.

The ^{1}H NMR spectra of the liquid fractions obtained at the first and seventh cycling tests under direct IH mode are presented in Fig. 9 and confirm the high stability of the carbon-based catalyst for operating waste plastic cracking into liquid hydrocarbon products with linear chains and a moderate isomerization of alkene derivatives according to the NMR analyses (Fig. S17-S30 in SI).

The percentage of the different hydrocarbon fractions obtained at various reaction durations using model HDPE is summarized in Table 3. It is worth to note that the ratio of aromatic versus aliphatic compounds is significantly decreased along the cycling tests switching from 7/93 wt %/wt% to 1/99 wt%/wt%. Such results are quite intriguing and seem to indicate that some active centers involved in the production of aromatic compounds are inhibited on the MESOC+ catalyst as a function of cycling tests. It is expected that the aromatic compounds could be formed at the beginning of the cycling tests on some residual oxygenated functional groups, localized within the porosity of the carbon material with low acidic property, and such acidic centers being gradually extinguished as a function of the cycling tests as part of the porosity was blocked by some solid residue. After the long-term cycling tests the solid carbonaceous residue deposited on the carbon sample is amounted to about 26 wt% despite the cracking performance remains relatively stable. Such results pointed out the fact that the carbon SSA is not an important parameter for the pyrolysis process. Work is ongoing on other type of carbon catalyst in order to investigate in more detail such results.

3.2.3. *Stability tests on mixed polymers*

Generally, the non-sorted waste plastics are mostly constituted by a mixture of several polymers which render difficult their separation during mechanical recycling process. In this study, a mixture of HDPE and LDPE was evaluated for the chemical recycling on the same spent carbon catalyst after seven cycling tests with HDPE (140 g of HDPE converted per 6 g of catalyst). The results are presented in Fig. 10 as a function of additional cycling tests with model mixture polymers. The cracking of LDPE alone yields a relatively high fraction of liquid with short and medium carbon chain as shown in Fig. 10 (noted LDPE#10). Such results can be explained by the fact that LDPE contains more branched chains along the polymer backbone which could be easily breaks down into short chain hydrocarbons. Adding LDPE into HDPE, regardless the relative concentration of each polymer, significantly improve the cracking process leading to higher fraction of short-chain hydrocarbons as depicted in Fig. 10. Such results could be explained by some synergistic effect between the two polymers vapors on the carbon cracking site. After cycling tests with different mixture of HDPE and LDPE, the test carrying out on the spent catalyst with the LDPE alone shows a net difference in terms of product formation by comparison to the colloidal mixture obtained with HDPE where only short-chain hydrocarbons were produced (Fig. 10). The return test using HDPE (Cycle#14 in Fig. 10) confirms the high stability of the catalyst for the cracking of model waste plastic into liquid hydrocarbon.

3.2.4. *Energy consumption*

The energy required for running the PTF process, either under direct IH or indirect Joule heating, was monitored by a clamp-on current probe. According to the results, IH mode requires more energy input during the reaction compared to the Joule heating despite this later consume more energy during the heating phase to reach the reaction temperature due to its high inertia. The ratio of the energy consumption

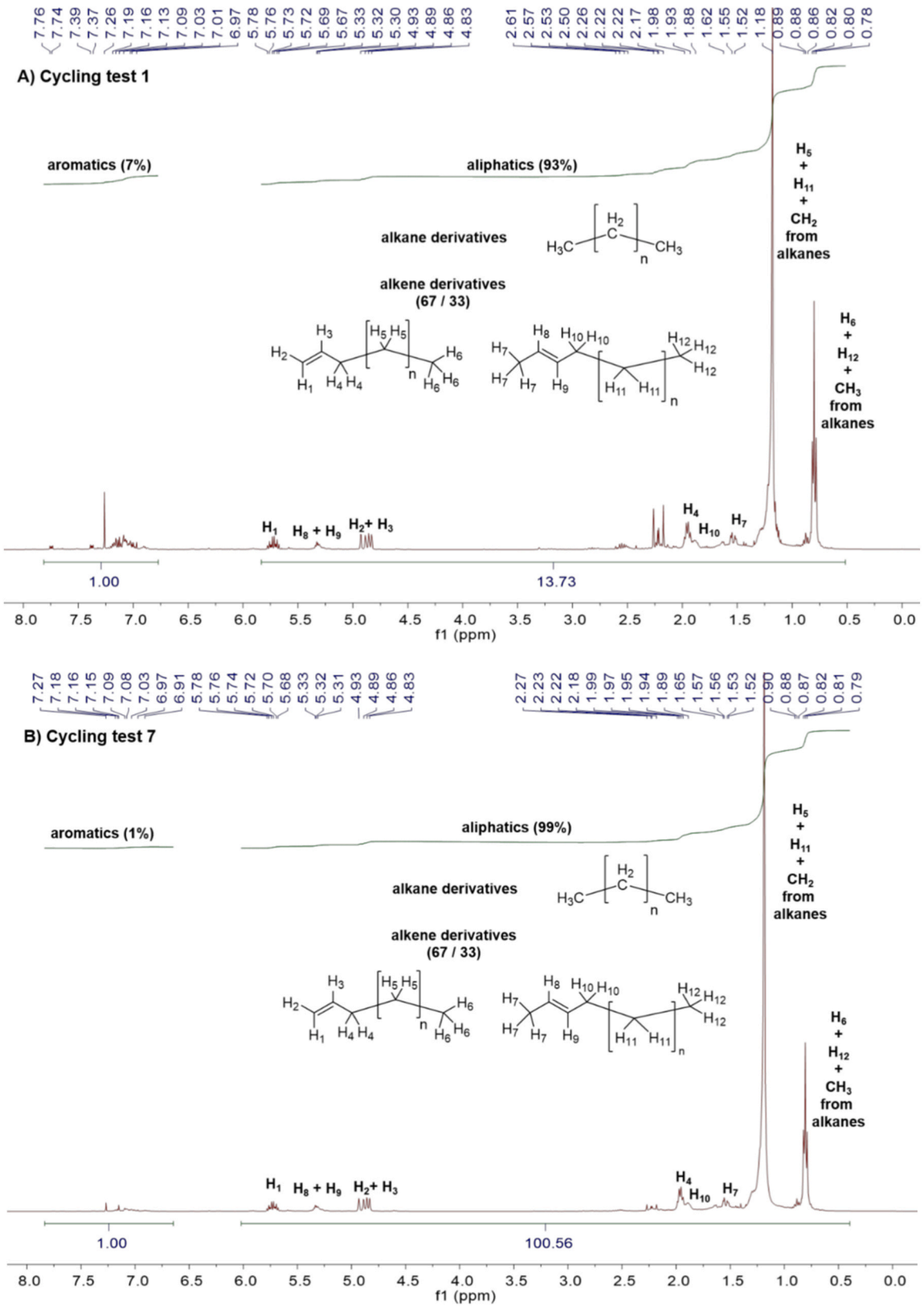

Fig. 9. ^{1}H NMR spectra of the liquid fraction obtained as a function of the polymer converted (in g) on the MESOC+ −3 catalyst operated under direct IH mode at 500 °C. Reaction conditions: mixed polymer weight feeding = 10 g. h^{-1} with discontinuous feeding, MESOC+ weight = 3 g (with an apparent volume of X cm^3), reactor diameter = 26 mm, argon flow rate = 30 mL. min^{-1}, HDPE vaporization at the first stage with an electric oven set at 450 °C. The liquid fraction was condensed in a trap keep at 10 °C using an external ice bath.

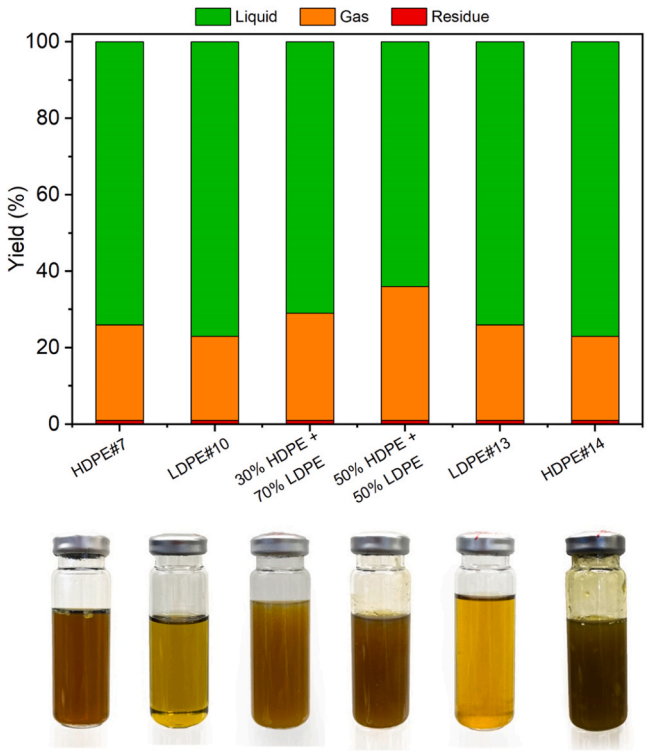

Fig. 10. Cycling tests for the plastic-to-Fuels (PTF) process using reference LDPE and mixed model polymers (HDPE and LDPE) on 3 mm pellets of MESOC+ material under direct induction heating mode at 500 °C. Reaction conditions: mixed polymers weight feeding = 10 g. h^{-1} with discontinuous feeding, MESOC+ weight = 6 g, reactor diameter = 26 mm, argon flow rate = 30 mL. min^{-1}, HDPE-LDPE vaporization at the first stage with an electric oven set at 450 °C. The liquid fraction was condensed in a trap keep at 10 °C using an external ice bath. Each cycle corresponding to 20 g of LDPE or a mixture of LDPE and HDPE passed through the catalyst bed.

between the two heating modes is $E_{IH}/E_{JH} = 1.9$. Such different in terms of energy input could be explained by several facts: (i) in our induction heated system the catalyst bed is not isolated from the surrounding atmosphere and is in direct contact with the induction coil localized few millimeters away (see SI). In such configuration the heat loss through exchange between the catalyst bed and the cold reactor wall in contact with the surrounding medium should be high which could explain the higher energy consumption for the induction mode vs the indirect Joule heating (commercial oven with high insulated ceramic shield). In addition, the coupling between the catalyst and the inductor remains low for the moment, around 3%, which could also explain the high energy consumption.

In order to improve such coupling efficiency further experiments will be conducted by modifying the electrical conductivity of the carbon sample (doped with higher conductor) as well as the dimension of the induction coil. It is expected that such changes will greatly contribute to the reduction of the overall energy input for the process and to improve the energy cost effectiveness of the process. In induction heating, a skin-effect phenomenon refers to the non-uniform distribution of the induced eddy currents within the susceptor material. Accordingly, the induced currents have a tendency to crowd toward the surface layers of the susceptor. The effective layers where current flow is concentrated is called *skin depth (δ)*, which can be expressed by the conductivity (σ, S/m), magnetic permeability (μ, H/m) and the frequency of current (f, Hz) following Eq. 1. High frequency f results in a small skin depth δ and vice-versa. Depending on the ratio of this parameter and the inductance (L, H), the skin-effect phenomenon is determined. When $\delta/L >> 1$, the skin-effect phenomenon is weak; the susceptor seems to be transparent to the magnetic field, i.e. the magnetic field penetrates within all the susceptor without resistance and, as a consequence, no heat is generated within the catalyst bed. In contrast, when $\delta/L \leq 1$, skin-effect phenomenon could be clearly observed which significantly contributes to the heating of the whole catalyst bed.

$$\delta = \frac{1}{\sqrt{\pi\sigma\mu f}} \tag{1}$$

The skin depth δ is also an important parameter to determine the coupling efficiency of the induction heating system (η,%). Accordingly, the coupling efficiency of induction heating system (η) is calculated from the supplied power of the induction system (P_{Supply}, W) and the power induced on the susceptor material (P_{load}, W), Eq. 2. Where the power induced on the susceptor material (P_{load}) depends on the magnetic field (Hs), the *skin depth (δ),* conductivity (σ), F is the geometric coefficient of the susceptor, and *external surface (S) and geometry* of the susceptor, Eq. 3.

$$\eta = \frac{P_{Load}}{P_{Supply} + P_{Load}} \tag{2}$$

$$P_{Load} = \frac{H_s^2}{\sigma} F.S \tag{3}$$

The modification of the induction coil dimension will also allow one to use insulation layer to prevent excessive heat loss through radiative and direct exchange with the surrounding medium as discussed above.

4. Conclusion

In summary, carbon-based catalyst can be efficiently used as acidic- and metal-free catalyst for the catalytic cracking of model waste polyolefin under contactless induction heating to yield gaseous and liquid hydrocarbons fractions at mild reaction temperature, ≤ 500 °C. The high catalytic performance could be attributed to the efficient catalyst bed temperature stability thanks to the high heating rate of the induction setup which allows one to compensate the internal temperature loss during such high endothermic process. The same catalyst operated under indirect Joule heating required much higher temperature, i.e. ≥ 600 °C, to convert waste plastic into long-chain hydrocarbons. Such results were attributed to the inability of the indirect convection/conduction heating mode to maintain a stable temperature at the catalytic site for such highly endothermic reaction. The carbon-based catalyst also displayed an extremely high stability as a function of polymer weight converted per gram of catalyst (for model HDPE up to 24 $g_{HDPE}.g^{-1}_{catalyst}$) under induction heating. In addition, the catalyst remains highly stable during cycling tests with mixed polymers, i.e. HDPE and LDPE, which are a representative model of non-sorting waste plastics. The results obtained clearly evidence the high efficiency of such combined catalytic system, carbon and induction heating, for operating waste plastic recycling where high and stable catalytic activity was obtained on a single carbon-based catalyst under a simple setup powered by contactless direct induction heating using renewable energy. It is expected that such simple-to-use and fully electrical powered catalytic system could open up a new area for promoting plastic recycling system for industry. The results obtained provide an efficient and cost-effective route for waste plastic recycling and also as chemical storage means for renewable energy. In addition, carbon-based catalyst with low cost production could promote such chemical recycling process and represents a net advantage compared to the acid or metal catalysts used nowadays where deactivation occurred with cycling tests. Work is ongoing to check out the influence of the carbon-based catalyst structure and specific surface area on the selectivity of the process and also to investigate the influence of impurities present in the waste plastic feed.

CRediT authorship contribution statement

C.D.V., **L.T.P.**, and **J.M.N.** designed the experiments and assisted with data analysis. **C.D.V.** carried out the different experiments and wrote the manuscript. **C.M.** and **L.N.D.** carried out experimental and assisted with data analysis and wrote the manuscript. **C.P.** discussed the experiments, data analysis and wrote the manuscript. **H.B.** discussed the experiments and data analysis. **C.P.H.** design the experiments, provided experimental and theoretical guidance, wrote the manuscript, funding.

Declaration of Competing Interest

The authors declare the following financial interests/personal relationships which may be considered as potential competing interests: C. D.V., L.T.P., J.M.N., C.P., H.B. and C.P.H. have patent #EP22306835.4 pending to CNRS, University of Strasbourg, BlackLeaf SAS, Sicat SAS.

Acknowledgments

The authors would like to thank the SATT Conectus for supporting the project and also A. Liegeon, R. Gresser, and N. Knepper for helpful discussion. The SEM experiments were carried out by T. Romero at the SEM platform Cronenbourg of the ICPEES and IPCMS while the TEM experiments were carried out by Dr. L. Vidal at the TEM platform of IS2M. Dr. V. Papaefthimiou (ICPEES) is also gratefully acknowledged for performing XPS on the carbon catalyst. C. Mélart, Dr. X. H. Pham and Prof. G. Schlatter (ICPEES) and Dr. M. Dumont (EMDPI) are gratefully acknowledged for providing polymer raw materials and for technical discussion and help during the project.

Appendix A. Supporting information

Supplementary data associated with this article can be found in the online version at doi:10.1016/j.mtcata.2023.100028.

References

[1] H. Sardon, A.P. Dove, Plastics recycling with a difference, Science 360 (2018) 380–381, https://doi.org/10.1126/science.aat4997.
[2] R. Geyer, J.R. Jambeck, K.L. Law, Production, use, and fate of all plastics ever made, Sci. Adv. 3 (2017), e1700782, https://doi.org/10.1126/sciadv.1700782.
[3] J.-P. Lange, Managing plastic waste-sorting, recycling, disposal, and product redesign, ACS Sustain. Chem. Eng. 9 (2021) 15722–15738, https://doi.org/10.1021/acssuschemeng.1c05013.
[4] M. Chu, Y. Liu, X. Lou, Q. Zhang, J. Chen, Rational design of chemical catalysis for plastic recycling, ACS Catal. 12 (2022) 4659–4679, https://doi.org/10.1021/acscatal.2c01286.
[5] F. Zhang, M. Zeng, R.D. Yappert, J. Sun, Y.-H. Lee, A.M. LaPointe, B. Paters, M. M. Abu-Omar, S.L. Scott, Polyethylene upcycling to long-chain alkylaromatics by tandem hydrogenolysis/aromatization, Science 33370 (2020) 437–441, https://doi.org/10.1126/science.abc54.
[6] S. Liu, P.A. Kots, B.C. Vance, A. Danielson, D.G. Vlachos, Plastic waste to fuels by hydrocracking at mild conditions, Sci. Adv. 7 (2021) eabf8283, https://doi.org/10.1126/sciadv.abf828.
[7] M. Roosen, N. Mys, M. Kusenberg, P. Billen, A. Dumoulin, J. Dewulf, K.M. Van Geem, K. Ragaert, S. De Meester, Detailed analysis of the composition of selected plastic packaging waste products and its implications for mechanical and thermochemical recycling, Environ. Sci. Technol. 54 (2020) 13282–13293, https://doi.org/10.1021/acs.est.0c03371.
[8] A. Somoza-Tornos, A. Gonzalez-Garay, C. Pozo, M. Graelles, A. Espuna, G. Guillen-Gosalbez, Realizing the potential high benefits of circular economy in the chemical industry: ethylene monomer recovery via polyethylene pyrolysis, ACS Sustain. Chem. Eng. 8 (2020) 3561–3572, https://doi.org/10.1021/acssuschemeng.9b04835.
[9] R. Meys, A. Katelhon, M. Bachmann, B. Winter, C. Zibunas, S. Suh, A. Bardow, Achieving net-zero greenhouse gas emission plastic by a circular carbon economy, Science 374 (2021) 71–76, https://doi.org/10.1126/science.abg985.
[10] C. Jehanno, J.W. Alty, M. Roosen, S. De Meester, A.P. Dove, E.Y.X. Chen, F. A. Leibfarth, H. Sardon, Critical advances and future opportunities in upcycling commodity polymers, Nature 603 (2022) 803–814, https://doi.org/10.1038/s41586-021-04350-0.
[11] A.E. Schwarz, T.N. Lighart, D. Godoi Bizarro, P. De Wild, B. Vreugdenhil, T. van Harmelen, Plastic recycling in a circular economy; determining environmental performance through an LCA matrix model approach, Waste Manag. 121 (2021) 331–342, https://doi.org/10.1016/j.wasman.2020.12.020.
[12] J. Zheng, S. Suh, Strategies to reduce the global carbon footprint of plastics, Nat. Clim. Change 9 (2019) 374–378, https://doi.org/10.1038/s41558-019-0459-z.
[13] G. Fadillah, I. Fatimah, I. Sahroni, M.M. Musawwa, T.M.E. Mahlia, O. Mauraza, Recent progress in low-cost catalysts for pyrolysis of plastic waste to fuels, Catalysts 11 (2021) 837, https://doi.org/10.3390/catal11070837.
[14] J.E. Rorrer, C. Troyano-Valls, G.T. Beckhaw, Y. Roman-Leshkov, Hydrogenolysis of polypropylene and mixed polyolefin plastic waste over Ru/C to produce liquid alkanes, ACS Sustain. Chem. Eng. 9 (2021) 11661–11666, https://doi.org/10.1021/acssuschemeng.1c03786.
[15] X. Jiao, K. Zheng, Z. Hu, S. Zhu, Y. Sun, Y. Xie, Conversion of waste plastics into value-added carbonaceous fuels under mild conditions, Adv. Mater. 33 (2021) 2170398, https://doi.org/10.1002/adma.202005192.
[16] L. Jia, S. Evans, S.V.D. Linden, Motivating actions to mitigate plastic pollution, Nat. Commun. 10 (2019) 4582, https://doi.org/10.1038/s41467-019-12666-9.
[17] L.D. Ellis, N.A. Rorrer, K.P. Sullivan, M. Otto, J.E. McGeehan, Y. Roman-Leshkov, N. Wierckx, G.T. Beckham, Chemical and biological catalysis for plastics recycling and upcycling, Nat. Catal. 4 (2021) 5539–5556, https://doi.org/10.1038/s41929-021-00648-4.
[18] N. Zhou, L. Dai, Y. Lv, H. Li, W. Deng, F. Guo, P. Chen, H. Lei, R. Ruan, Catalytic pyrolysis of plastic wastes in a continuous microwave assisted pyrolysis system for fuel production, Chem. Eng. J. 418 (2021), 129412, https://doi.org/10.1016/j.cej.2021.129412.
[19] G. Lopez, M. Artetxe, M. Amutio, J. Bilbao, M. Olazar, Thermochemical routes for the valorization of waste polyolefinic plastics to produce fuels and chemicals. A review, Renew. Sustain. Energy Rev. 73 (2017) 346–368, https://doi.org/10.1016/j.rser.2017.01.142.
[20] K. Ding, S. Liu, Y. Huang, S. Liu, N. Zhou, P. Peng, Y. Wang, P.L. Chen, R.R. Ruan, Catalytic microwave-assisted pyrolysis of plastic waste over NiO and HY for gasoline-range hydrocarbons production, Energy Convers. Manag. 196 (2019) 1316–1325, https://doi.org/10.1016/j.enconman.2019.07.001.
[21] X. Zhang, H. Lei, G. Yadavalli, L. Zhu, Y. Wei, Y. Liu, Gasoline-range hydrocarbons produced from microwave-induced pyrolysis of low-density polyethylene over ZSM-5, Fuel 144 (2015) 33–42, https://doi.org/10.1016/j.fuel.2014.12.013.
[22] A. Lopez, I. de Marco, B.M. Caballero, A. Adrados, M.F. Laresgoiti, Deactivation and regeneration of ZSM-5 zeolite in catalytic pyrolysis of plastic wastes, Waste Manag 31 (20011) (1852-1858).
[23] L. Dai, N. Zhou, K. Cobb, P. Chen, Y. Wang, Y. Liu, R. Zou, H. Lei, B.A. Mohamed, Y. Cheng, R. Ruan, Insight into structure-performance relationship in the catalytic cracking of high density polyethylene, Appl. Catal. B: Environ. 318 (2023), 121835, https://doi.org/10.1016/j.apcatb.2022.121835.
[24] Y. Nakaji, M. Tamura, S. Miyaoka, S. Kumagai, M. Tanji, Y. Nakagawa, T. Yoshiokka, K. Tomishige, Low-temperature catalytic upgrading of waste polyolefinic plastics into liquid fuels and waxes, Appl. Catal. B: Environ. 285 (2021), 119805, https://doi.org/10.1016/j.apcatb.2020.119805.
[25] C.A. Mullen, C. Dorado, A.A. Boateng, Catalytic co-pyrolysis of switchgrass and polyethylene over HZSM-5: catalyst deactivation and coke formation, J. Anal. Appl. Pyrol. 129 (2018) 195–203, https://doi.org/10.1016/j.jaap.2017.11.012.
[26] B. Du, X. Chen, Y. Ling, T. Niu, W. Guan, J. Meng, H. Hu, C.-W. Tsang, C. Liang, Hydrogenolysis-isomerization of waste polyolefin plastics to multibranched liquid alkanes, ChemSusChem 16 (2023), e202202035, https://doi.org/10.1002/cssc.202202035.
[27] K. Sun, Q. Huang, X. Meng, Y. Chi, J. Yan, Catalytic pyrolysis of waste polyethylene into aromatics by H_3PO_4-activated carbon, Energy Fuels 32 (2018) 9772–9781, https://doi.org/10.1021/acs.energyfuels.8b02091.
[28] Y. Zhang, D. Duan, H. Lei, E. Villota, R. Ruan, Jet fuel production from waste plastics via catalytic pyrolysis with activated carbons, Appl. Energy 251 (2019), 113337, https://doi.org/10.1016/j.apenergy.2019.113337.
[29] C. Duong-Viet, C. Pham, C. Pham-Huu, L. Truong-Phuoc, J.-M. Nhut, H. Ba, Y. Lafue, S. Wambergue, Use of metal-free carbon material for converting plastic into C_2-C_4 olefins and/or hydrocarbons, under direct induction heating, and the method thereof. Eur. Pat. Appl. No. EP22306835.4, filed on August 24, 2022, assigned to the CNRS, University of Strasbourg, BlackLeaf SAS, and Sicat SARL, 2022.
[30] A. Bogaerts, G. Centi, V. Hessel, E. Rebrov, Challenges in unconventional catalysis, Catal. Today 420 (2023), 114180.
[31] J. Marbaix, N. Mille, L.-M. Lacroix, J.M. Asensio, P.-F. Fazzini, K. Soulantica, J. Carrey, B. Chaudret, Tuning the composition of FeCo nanoparticles heating agents for magnetically induced catalysis, ACS Appl. Nano Mater. 3 (2020) 3767–3778, https://doi.org/10.1021/acsanm.0c00444.
[32] H. Kreissl, J. Jin, S.H. Lin, D. Schüette, S. Störtte, N. Levin, B. Chaudret, A. J. Vorholt, A. Bordet, W. Leitner, Commercial Cu2Cr2O5 decorated with iron carbide nanoparticles as a multifunctional catalyst for magnetically induced continuous-flow hydrogenation of aromatic ketones, Angew. Chem. Int. Ed. 60 (2021) 26639–26646, https://doi.org/10.1002/anie.202107916.
[33] C. Cerezo-Navarrete, I.M. Marin, H. García-Miquel, A. Corma, B. Chaudret, L. M. Martínez-Prieto, Magnetically induced catalytic reduction of biomass-derived oxygenated compounds in water, ACS Catal. 12 (2022) 8462–8475, https://doi.org/10.1021/acscatal.2c01696.
[34] M. Marin, D. De Masi, L.M. Lacroix, P.F. Fazzini, P.W. van Leeuwen, J.M. Asensio, B. Chaudret, Hydrodeoxygenation and hydrogenolysis of biomass-based materials using FeNi catalysts and magnetic induction, Green. Chem. 23 (2021) 2025–2036, https://doi.org/10.1039/D0GC03495A.
[35] L. Truong-Phuoc, C. Duong-Viet, G. Tuci, A. Rossin, J.-M. Nhut, W. Baaziz, O. Ersen, M. Arab, A. Jourdan, G. Giambastiani, C. Pham-Huu, Graphite felt-sandwiched Ni/SiC catalysts for the induction versus joule-heated sabatier reaction: assessing the catalyst temperature at the nanoscale, ACS Sustain. Chem. Eng. 10 (2022) 622–632, https://doi.org/10.1021/acssuschemeng.1c07217.

[36] C. Niether, S. Faure, A. Bordet, J. Deseure, M. Chatenet, J. Carrey, B. Chaudret, A. Rouet, Improved water electrolysis using magnetic heating of FeC–Ni core–shell nanoparticle, Nat. Energy 3 (2018) 476–483, https://doi.org/10.1038/s41560-018-0132-1.

[37] S.-H. Lin, W. Hetaba, B. Chaudret, W. Leitner, A. Bordet, Copper-decorated iron carbide nanoparticles heated by magnetic induction as adaptive multifunctional catalysts for the selective hydrodeoxygenation of aldehydes, Adv. Energy Mater. 12 (2022) 2270173, https://doi.org/10.1002/aenm.202201783.

[38] Z. Luo, X. Zhu, Y. Ma, K. Gong, X. Zhu, Alternating magnetic field initiated catalytic deconstruction of medical waste to produce hydrogen-rich gases and graphite, Cell Rep. Phys. Sci. 3 (2022), 100934, https://doi.org/10.1016/j.xcrp.2022.100934.

[39] W. Wang, C. Duong-Viet, G. Tuci, J.-M. Nhut, G. Giambastiani, C. Pham-Huu, Induction heating: an enabling technology for the heat management in catalytic processes (and references herein), ACS Catal. 9 (2019) 7921–7935, https://doi.org/10.1021/acscatal.9b02471.

[40] W. Wang, C. Duong-Viet, Z. Xu, H. Ba, G. Tuci, G. Giambastiani, Y. Liu, T. Truong-Huu, J.-M. Nhut, C. Pham-Huu, CO_2 methanation under dynamic operational mode using nickel nanoparticles decorated carbon felt (Ni/OCF) combined with inductive heating, Catal. Today 357 (2020) 214–220, https://doi.org/10.1016/j.cattod.2019.02.050.

[41] M.H. Nguyen, M.C. Phan, S. Liu, C. Pham-Huu, L. Nguyen-Dinh, Radiofrequency induction heating powered low-temperature catalytic CO_2 conversion via bi-reforming of methane, Chem. Eng. J. 430 (2022), 132934, https://doi.org/10.1016/j.cej.2021.132934.

[42] W. Wang, C. Duong-Viet, T. Truong-Huu, T. Truong-Huu, M.H. Nguyen, L. Nguyen-Dinh, Y. Liu, C. Pham-Huu, Improving catalytic performance by induction heating: selective oxidation of H_2S on nitrogen-doped carbon catalyst as model reaction, N. J. Chem. 47 (2023) 1105–1116, https://doi.org/10.1039/D2NJ04897C.

[43] W. Wang, C. Cuong Duong-Viet, L. Truong-Phuoc, J.-M. Nhut, L. Vidal, C. Pham-Huu, Activated carbon supported nickel catalyst for selective CO_2 hydrogenation to synthetic methane under contactless induction heating, Catal. Today 418 (2023), 114073, https://doi.org/10.1016/j.cattod.2023.114073.

[44] Z.J. Schiffer, K. Manthiram, Electrification and decarbonization of the chemical industry, Joule 1 (2017) 10–14, https://doi.org/10.1016/j.joule.2017.07.008.

[45] Y. Miao, Y. Zhao, G.I.N. Waterhouse, R. Shi, L.-Z. Wu, T. Zhang, Photothermal recycling of waste polyolefin plastics into liquid fuels with high selectivity under solvent-free conditions, Nat. Commun. 14 (2023) 4242, https://doi.org/10.1038/s41467-023-40005-6.

[46] H. Zhou, Y. Ren, Z. Li, M. Xu, Y. Wang, R. Ge, X. Kong, L. Zheng, H. Duan, Electrocatalytic upcycling of polyethylene terephthalate to commodity chemicals and H_2 fuel, Nat. Commun. 12 (2021) 4679, https://doi.org/10.1038/s41467-021-25048-x.

[47] C.-C. Chen, L. Dai, L. Ma, R.T. Guo, Enzymatic degradation of plant biomass and synthetic polymers, Nat. Rev. Chem. 4 (2020) 114–126, https://doi.org/10.1038/s41570-020-0163-6.

[48] Y. Wang, D.C. Alsmeyer, R.L. McCreery, Raman spectroscopy of carbon materials: structural basis of observed spectra, Chem. Mater. 2 (1990) 557–563, https://doi.org/10.1021/cm00011a018.

[49] A. Sadezky, H. Muckenhuber, H. Grothe, R. Niessner, U. Pöschl, Raman microspectroscopy of soot and related carbonaceous materials spectral analysis and structural information, Carbon 43 (2005) 1731–1742, https://doi.org/10.1016/j.carbon.2005.02.018.

[50] X.S. Zhang, H.W. Lei, J. Zhu, M. Qian, G. Yadavalli, J. Wu, S. Chen, From plastics to jet fuel range alkanes via combined catalytic conversions, Fuel 188 (2017) 28–38, https://doi.org/10.1016/j.fuel.2016.10.015.

[51] I. Julian, H. Ramirez, J.L. Hueso, R. Mallada, J. Santamaria, Non-oxidative methane conversion in microwave-assisted structured reactors, Chem. Eng. J. 377 (2019), 119764, https://doi.org/10.1016/j.cej.2018.08.150.

[52] V.P. Dotsenko, M. Bellusci, A. Masi, D. Pietrogiacomi, F. Varsano, Improving the performances of supported NiCo catalyst for reforming of methane powered by magnetic induction, Catal. Today 418 (2023), 114049, https://doi.org/10.1016/j.cattod.2023.114049.

[53] H. Chen, K. Wan, Y. Zhang, Y. Wang, Waste to wealth: chemical recycling and chemical upcycling of waste plastics for a great future, ChemSusChem 14 (2021) 4123–4136, https://doi.org/10.1002/cssc.202100652.

[54] X. Jie, W. Li, D. Slocombe, Y. Gao, I. Banerjee, S. Gonzalez-Cortes, B. Yao, H. AlMegren, S. Alshiri, J. Dilworth, J. Thomas, T. Xiao, P. Edward, Microwave-initiated catalytic deconstruction of plastic waste into hydrogen and high-value carbons, Nat. Catal. 3 (2020) 902–912, https://doi.org/10.1038/s41929-020-00518-5.

[55] A. Malhotra, W. Chen, H. Goyal, P.J. Plaza-Gonzalez, I. Julian, J.M. Catala-Civera, D.G. Vlachos, Temperature homogeneity under selective and localized microwave heating in structured flow reactors, Ind. Eng. Chem. Res. 60 (2021) 6835–6847, https://doi.org/10.1021/acs.iecr.0c05580.

[56] A. Ramirez, J.L. Hueso, M. Abian, M.U. Alzueta, R. Mallada, J. Santamaria, Escaping undesired gas-phase chemistry: microwave-driven selectivity enhancement in heterogeneous catalytic reactions, Sci. Adv. 5 (2019) eaau99000.

[57] P.D. Muley, C. Henkel, K.K. Abdollahi, D. Boldor, Pyrolysis and catalytic upgrading of pinewood sawdust using an induction heating reactor, Energy Fuel 29 (2015) 7375–7385, https://doi.org/10.1021/acs.energyfuels.5b01878.

[58] M. Abu-Laban, P.D. Muley, D.J. Hayes, D. Boldor, Ex-situ up-conversion of biomass pyrolysis bio-oil vapors using Pt/Al_2O_3 nanostructured catalyst synergistically heated with steel balls via induction, Catal. Today 291 (2017) 3–12, https://doi.org/10.1016/j.cattod.2017.01.010.

[59] J. Bursavich, M. Abu-Lalan, P.D. Muley, D. Boldor, D.J. Hayes, Thermal performance and surface analysis of steel-supported platinum nanoparticles designed for bio-oil catalytic upconversion during radio frequency-based inductive heating, Energ. Convers. Manag. 183 (2019) 689–697, https://doi.org/10.1016/j.enconman.2019.01.025.

[60] L. Wu, H. Ma, Z. Yan, Q. Xu, Z. Li, Improving catalyst performance of Ni-CaO-C to enhance H_2 production from biomass steam gasification through induction heating technology, Energy Convers. Manag. 270 (2022) 1116242, https://doi.org/10.1016/j.enconman.2022.116242.

[61] A. Ramirez, J.L. Hueso, R. Mallada, J. Santamaria, Microwave-activated structured reactors to maximize propylene selectivity in the oxidative dehydrogenation of propane, Chem. Eng. J. 393 (2020), 124746, https://doi.org/10.1016/j.cej.2020.124746.